Polymer 52 (2011) 2016–2024

Contents lists available at ScienceDirect

Polymer

journal homepage: www.elsevier.com/locate/polymer

Multifunctional fiberglass-reinforced PMMA-$BaTiO_3$ structural/dielectric composites

Eduard A. Stefanescu, Xiaoli Tan, Zhiqun Lin, Nicola Bowler, Michael R. Kessler*

Department of Materials Science and Engineering, Iowa State University, 2220 Hoover Hall, Ames, IA 50011, USA

ARTICLE INFO

Article history:
Received 23 November 2010
Received in revised form
23 February 2011
Accepted 28 February 2011
Available online 8 March 2011

Keywords:
Dielectric
Multifunctional
Polymer composite

ABSTRACT

Fiberglass-reinforced polymer composites were investigated for potential use as structural dielectrics in multifunctional capacitors that require simultaneous excellent mechanical properties and good energy storage characteristics. Composites were fabricated employing poly(methyl methacrylate), PMMA, as the structural matrix. While barium titanate ($BaTiO_3$) nanopowder was added to the composites for its high room temperature dielectric constant, fiberglass was employed to confer high stiffness. A conductive polymer blend of poly (3,4-ethylenedioxythiophene) and polystyrene sulfonate (PEDOT:PSS) was used to coat the $BaTiO_3$ nanoparticles with the purpose of further elevating the dielectric constant of the resultant PMMA-composites. FTIR spectroscopy, TGA and SEM measurements were conducted to prove the successful coating of $BaTiO_3$ nanoparticles with the PEDOT:PSS blend. TEM measurements revealed a good dispersion of coated nanoparticles throughout the PMMA matrix. The fiberglass-reinforced-PMMA composites containing neat and coated $BaTiO_3$ were found to exhibit excellent stiffness. In addition, the use of PEDOT:PSS in conjunction with $BaTiO_3$ was observed to improve the dielectric constant of the composites. Finally, the dielectric constant of the structural composites was found to vary only slightly with temperature.

1. Introduction

In recent years substantial efforts have been dedicated to finding new alternatives for performance, weight and volume improvements in batteries and capacitors [1–4]. Such efforts are generated in part by the ever-growing demand for energy storage in a wide variety of emerging applications, including hybrid ground vehicles, airplanes and space shuttles. In the most common electronic devices present today on the market the majority of circuit components are passive, accounting for more than 80% of printed wired surface area [1]. In addition, capacitors, especially those with high capacitances, are among the largest passive electronic components. A recent study indicated that in 2008 approximately 90% (by volume) of the capacitor market was dominated by the ceramic capacitors [5]. While commercial ceramic capacitors are typically employed where small sizes along with high capacitances and insulation resistances are required, they are not intended for precision applications due to high variations in the capacitance with temperature [2]. In contrast, polymer film capacitors are predominantly used in applications requiring low dielectric absorption and loss factors over a wide temperature range [2]. However, polymer film capacitors are characterized by smaller capacitances due to their lower dielectric constants compared to the ceramic counterparts. We hypothesize that polymer composites obtained through the addition of ceramic powders into polymeric matrixes, can result in improved dielectric candidates for capacitors with an enlarged spectrum of applications. The spectrum of applications can be even further expanded to structural components when such capacitors are designed with structural characteristics, such as high-strength and stiffness.

Fiberglass-reinforced polymer composites have been extensively studied in past decades, primarily for their high specific strength and stiffness [6,7]. Such fiberglass-reinforced materials are typically employed in applications where fatigue durability and high fracture toughness are important requirements [6]. Several reports have previously focused on the fabrication and analysis of poly(methyl methacrylate), PMMA-based materials containing fiberglass as reinforcement [8,9]. PMMA is a high-strength, amorphous polymer possessing good dimensional stability and outdoor wearing properties. Owing to these characteristics, PMMA is among the most heavily studied polymers for nano- and micro-composite fabrications [10–19]. Various in situ [10,12,13,15,16] and/or ex-situ [14–16,19] approaches have been used to disperse different fillers in PMMA matrixes. Because of its high optical transparency PMMA is commonly employed in various applications as a low-density and

* Corresponding author. Tel.: +1 515 294 3101.
E-mail address: mkessler@iastate.edu (M.R. Kessler).

0032-3861/$ – see front matter © 2011 Elsevier Ltd. All rights reserved.
doi:10.1016/j.polymer.2011.02.050

shatter-resistant alternative to glass. Additionally, the high stiffness of PMMA, along with its biocompatibility, renders it the matrix of choice in cements for bone-substitute applications [20,21]. Despite its exceptional mechanical behavior, PMMA exhibits a rather low dielectric constant, with values between 3 and 8, depending on molecular weight and testing frequency [15,18,22].

Barium titanate, $BaTiO_3$, is a ceramic material with a perovskite crystal structure characterized by excellent ferroelectric and piezoelectric properties [5,14,23–25]. The ferroelectricity of this ceramic causes very high dielectric constants (ϵ'), with the highest reported ϵ' value reaching 10,000 [5]. Due to its very high ϵ', $BaTiO_3$ has been extensively employed in the fabrication of multilayer ceramic capacitors [24]. In recent years $BaTiO_3$ has been utilized for composite preparation in conjunction with various polymers, including PMMA [14,23,24,26]. It has been suggested that the surface functionalization of $BaTiO_3$ with various chemicals can significantly improve the interactions between $BaTiO_3$ and the polymer matrix [14,26].

Poly (3,4-ethylenedioxythiophene) (PEDOT) has been a heavily studied conductive polymer during the past decade [27–32]. The intense interest in PEDOT-containing materials arises mainly from the remarkable electron-conducting properties of this polymer, coupled with its high chemical stability, low-density and relatively low cost [27,32]. PEDOT is often employed in conjunction with sulfonated polymers such as polystyrene sulfonate (PSS). The role of PSS in PEDOT:PSS mixtures is two-fold: on one hand, PSS provides the charge-balancing counter ions necessary for the stabilization of the p-doped PEDOT; on the other hand, PSS promotes the homogeneous dispersion of PEDOT chains in water, allowing for the production and commercialization of PEDOT:PSS aqueous solutions [31]. When utilized from aqueous solutions, PEDOT has an excellent film-forming ability, which allows for coating various powdery and/or non-powdery materials; these materials include carbon nanotubes (CNT) [27], barium ferrite (BaFe) [32], and cellulose acetate [28].

Herein, we focused on PMMA-fiberglass structural dielectrics containing neat or PEDOT:PSS-coated $BaTiO_3$ particles, for potential use in multifunctional capacitors that require superior stiffness and energy storage characteristics. The multifunctional capacitors could be potentially employed as substitutes for static load-carrying components in traditional structures (e.g., hybrid vehicles or airplanes) with the purpose of reducing the overall system weight and/or volume.

2. Experimental

2.1. Materials

All chemicals were used as received from their vendors, without any additional purification. PMMA (MW = 996,000 g/mol, inherent viscosity = 1.25 dL/g) and PEDOT:PSS (1.3 wt% dispersion in H_2O) were purchased from Sigma–Aldrich Corporation (St. Louis, MO). $BaTiO_3$ nanoparticles (NanOxide™, HPB 1000, <100 nm, lot # BTA040120MC) were obtained from TPL Inc (Albuquerque, NM). The fiberglass fabric (bi-directional E-Glass, thickness 0.008") was obtained from Fiber Glast Developments Corporation (Brookville, OH). Chloroform (HPLC grade, d = 1.49 g/mL) was purchased from Fisher Scientific (Hampton, NH).

2.2. Coating of $BaTiO_3$ particles

$BaTiO_3$ nanoparticles (13 g) were added to a flask containing 10 mL PEDOT:PSS aqueous solution (dark blue color). The ceramic particles were vigorously dispersed via probe sonication for a period of 5 min. Following sonication, the flask containing the aqueous dispersion was placed on a hot plate at 80 °C, and the entire system was gently stirred overnight with a magnetic stir bar. After the entire amount of water was evaporated, the $BaTiO_3$ particles (white in the neat form) exhibited a blue color, indicating an effective coating. The coated particles were additionally dried in an oven at 80 °C overnight and stored in a tightly capped vial. The calculated amount of PEDOT:PSS in the resultant coated $BaTiO_3$ particles was ≈1 wt.%.

2.3. PMMA-based composites fabrication

The PMMA powder was initially dissolved in chloroform in a mass ratio PMMA:$CHCl_3$ of 1:9. Following dissolution either neat or coated $BaTiO_3$ particles were added to the polymer solution and homogeneously dispersed employing a probe sonicator. Each of the resultant dispersions was manually spread with a spatula on each of the two sides of a fiberglass patch, previously cut to desired dimensions (see schematic in Fig. 4). In between individual spreads the solvent was evaporated on a hot plate at 50 °C. Subsequently, the resultant polymer composites were compression-molded in a hot press at 200 °C at pressures >200 PSI (>14 atm). The pressure was removed only after the press-plates were cooled back to room temperature. Following this method three distinct polymer composites were fabricated (Fig. 4) with the compositions described in Table 1.

2.4. Characterization of nanocomposites

Dielectric properties of the samples were characterized using a Novocontrol dielectric spectrometer (Novocontrol Technologies GmBh, Hundsangen, Germany). Frequency sweeps were performed from 1 Hz to 1 MHz. The dielectric constant and tan δ values were recorded with the WinDeta software. Thermogravimetric analysis (TGA) was performed with a TA Instruments (New Castle, DE) Q50 thermobalance. Neat and coated $BaTiO_3$ powders were subjected to TGA measurements in air at a heating rate of 10 °C/min, whereas polymer composite samples were analyzed in air with a heating rate of 20 °C/min. Differential scanning calorimetry (DSC) measurements were conducted using a TA Instruments Q20 analyzer at a heating rate of 10 °C/min. Dynamic mechanical analysis (DMA) was conducted on a TA Instruments Q800 analyzer

Table 1
Sample composition and dielectric breakdown strengths.

Sample name	Composition (grams)				Dielectric breakdown strength[b] (kV/cm)
	Fiberglass	PMMA	Neat $BaTiO_3$	Coated $BaTiO_3$[a]	
FG-PMMA	4	3	N/A	N/A	158 (±14%)
FG-PMMA-BT	4	3	3	N/A	139 (±20%)
FG-PMMA-BT(PEDOT:PSS)	4	3	N/A	3	76 (±17%)

[a] $BaTiO_3$ coated with PEDOT:PSS.
[b] Breakdown strength values were calculated as the mean of five measured values.

at a heating rate of 3 °C/min. Tension tests were performed with a Universal Testing Machine (Instron 5569) on ASTM type V samples at a crosshead speed of 1 mm/min. Dielectric breakdown measurements were performed on an Instron/CEAST (Norwood, MA) dielectric rigidity apparatus at a frequency of 50–60 Hz, a voltage ramp rate of 0.1 kV/s and a current intensity of 10 mA. Scanning electron microscopy (SEM) was carried out using a FEI Quanta 250 field emission microscope operated under high vacuum in the secondary-electrons mode. Sample preparation for SEM included sputter coating the samples with a thin layer of gold. Transmission electron microscopy (TEM) was performed using a JEOL 2100 200 kV microscope. The samples were prepared for TEM imaging by ultramicrotomy. Multiple discrete sections were examined by both SEM and TEM and only representative images are presented here. Duplicate measurements showed excellent reproducibility of all measured parameters.

3. Results and discussion

3.1. Coating of $BaTiO_3$ particles

The coating of $BaTiO_3$ particles was performed, on one hand, to improve the interaction between the inorganic particles with the organic polymer matrix and, on the other hand, to directly impact the dielectric properties of the resultant polymer composites. To verify the effectiveness of the coating process, a series of FTIR, TGA and SEM measurements were performed on both the non-coated and the coated $BaTiO_3$ particles. Fig. 1 shows the FTIR spectra from the PEDOT:PSS, neat $BaTiO_3$ and coated $BaTiO_3$ samples at room temperature. In the PEDOT:PSS curve a multitude of peaks is visible between 950 and 1750 cm^{-1}. The small peak at 976 is attributed to the C–S bond vibrations in the thiophene rings of PEDOT [27]. The peak at 1085 cm^{-1} is assigned to the stretching modes of the C–O–C bonds in PEDOT, but the broad shoulder observed to the right of the peak is expected to contain the component from the bending of the C–H bond in the aromatic rings of PSS (bond previously observed at 1007 cm^{-1} for PSS alone) [27]. Additionally, the broad peak at 1190 cm^{-1} is representative for the symmetric vibrations of the $-SO_3$ group in PSS. The broad short peak at 1324 cm^{-1} (not indicated with an arrow) and the multitude of peaks visible around 1540 cm^{-1}can be attributed to the C–C and C=C stretching of qunoidal structure and stretching of thiophene rings in PEDOT, respectively [32]. The larger peak at 1637 cm^{-1}may be attributed to skeletal vibrations involving stretching of the less strained C=C bonds from the aromatic rings of PSS. On the other hand, for the neat $BaTiO_3$, the two wide bands at 428 $cm^{-1}$and 565 cm^{-1} are characteristic to this type of ceramic and have been previously reported [23–25]. Furthermore, the small peak at 860 cm^{-1}corresponds to the Ti–O stretching modes [23], and the peaks at 1440 $cm^{-1}$and 1630 cm^{-1} are attributed to the symmetric and asymmetric stretching vibrations of carboxylic groups [25]. Finally, the FTIR curve corresponding to the PEDOT:PSS-coated $BaTiO_3$ sample is observed to exhibit contributions from both the neat $BaTiO_3$ and the neat PEDOT:PSS, indicating a successful deposition of the polymeric blend at the surface of the ceramic nanoparticles. A schematic showing the possible physical interactions between the polymeric chains and $BaTiO_3$ particles is shown in the "supporting information".

TGA measurements were performed primarily to determine the actual amount of PEDOT:PSS polymer deposited at the surface of $BaTiO_3$ particles. Fig. 2 shows the TGA curves obtained from the coated and neat $BaTiO_3$ particles. The inset in Fig. 2 displays the physical appearance of the inorganic particles prior to, and after the coating. Although the profile of the two TGA curves is not significantly different, in the case of the curve corresponding to the PEDOT:PSS-coated $BaTiO_3$ particles a more pronounced drop can be observed for the temperature range between 300 and 500 °C. It is apparent that upon heating in air from room temperature to 800 °C the neat $BaTiO_3$ particles lose 1.5% of their initial weight. On the other hand, the PEDOT:PSS-coated $BaTiO_3$ particles lose 2.4% of their initial weight on being subjected to an identical decomposition program. The difference in the lost mass percentage (0.9%) between the two samples is attributable to the presence of the polymeric blend coating at the surface of the ceramic particles. This practical value of 0.9 wt.% PEDOT:PSS is in a good agreement with the calculated value of 1 wt.%. Duplicate measurements showed excellent reproducibility of these results. Regarding the physical appearance of the $BaTiO_3$ particles, it is evident that prior to coating the neat inorganic powder is bright white (left image in the inset). Following the PEDOT:PSS deposition process the $BaTiO_3$ particles exhibit a light-blue color (right image in the inset), which resembles the color of PEDOT:PSS, indicating successful coating of PEDOT:PSS on the surface of $BaTiO_3$ particles.

SEM measurements were carried out on the neat and coated powders to uncover morphological differences between the two systems at the nanometer and micrometer scales. Fig. 3 shows the SEM micrographs at two magnifications for the neat $BaTiO_3$ (a and b) and (PEDOT:PSS)-coated $BaTiO_3$ (c and d). The low magnification image for neat $BaTiO_3$ (a) reveals that in the powdery form the inorganic nanoparticles coalesce together and form approximately spherical aggregates with diameters ranging from submicron to about 20 μm. The high magnification image for neat $BaTiO_3$ (b)

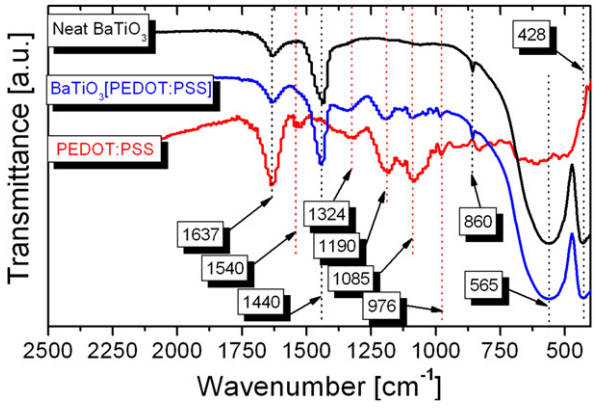

Fig. 1. FT IR spectra from the PEDOT:PSS, neat $BaTiO_3$ and PEDOT:PSS-coated $BaTiO_3$ samples at room temperature.

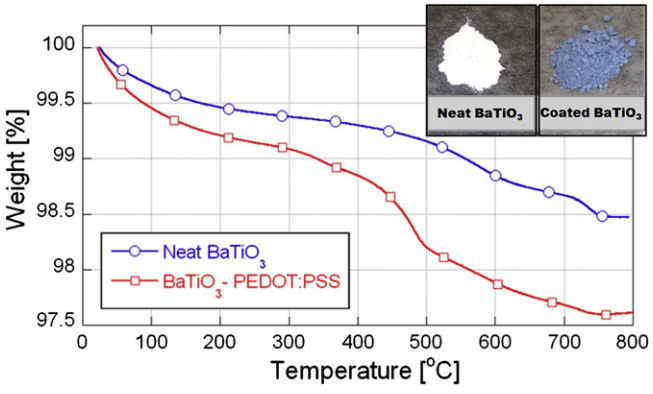

Fig. 2. TGA traces from $BaTiO_3$ and (PEDOT:PSS)-coated $BaTiO_3$ heated in air. The heating rate was 10 °C/min.

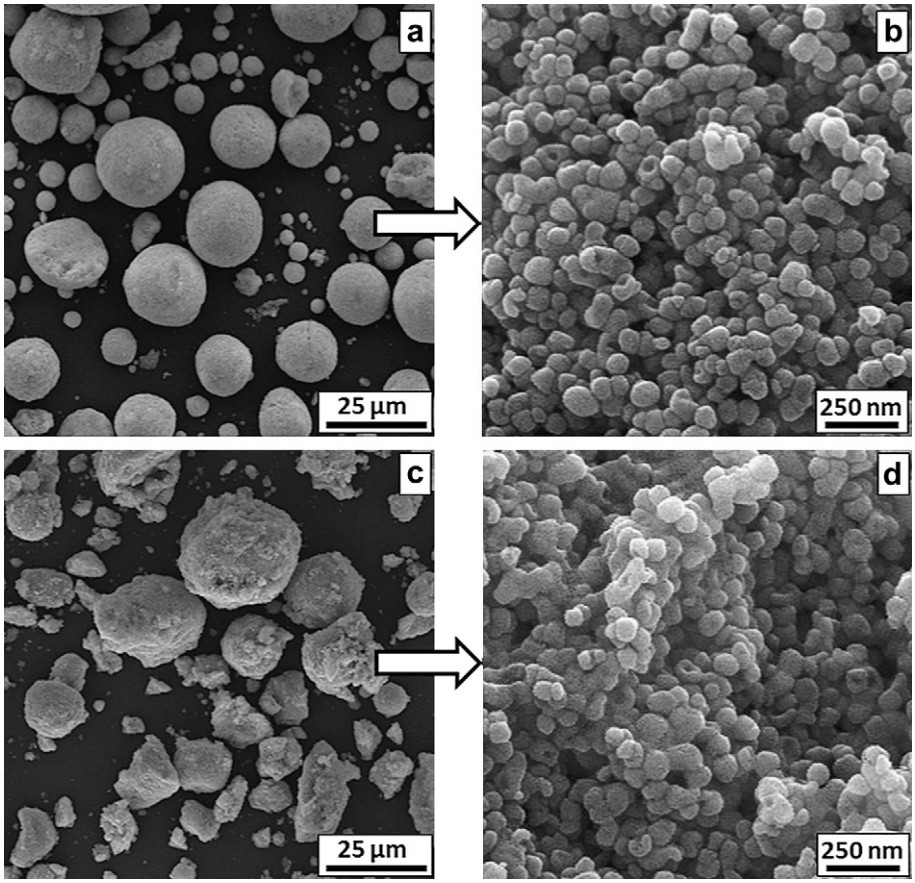

Fig. 3. SEM images at two distinct magnifications for the neat $BaTiO_3$ (a and b) and (PEDOT:PSS)-coated $BaTiO_3$ (c and d).

shows that the ceramic nanoparticles, making up the spherical aggregates, are in direct contact with each other. On the other hand, for the (PEDOT:PSS)-coated $BaTiO_3$ system, the low magnification image (c) reveals that the micrometric aggregates have random shapes with dimensions up to 25 μm. Furthermore, in the high magnification image for the coated powder (d) the nanostructures appear to be interconnected and covered in the polymer blanket, indicating a successful coating even at the nanoscale. Multiple powder-covered areas were examined by SEM and only representative images are presented here for the two systems. These weak agglomerations shown in Fig. 3 are introduced during the drying step in the manufacturing process and are easily broken up by ultrasonication as will be shown later.

3.2. PMMA-composites: fabrication and morphology

Subsequently, the three polymer composites described in Table 1 were prepared employing a solution-spreading method followed by compression-molding, as described in Section 2. The schematic diagram in Fig. 4 illustrates the method employed for composite fabrication. Photographs of the three fiberglass-PMMA composites are also shown at the bottom of Fig. 4. In this process the polymeric dispersion containing the ceramic particles is shear-spread with a spatula, resulting in uniform coating of the fiberglass fabric. The final compression-molding step leads to the formation of a compact, solvent-free composite material with excellent thermo-mechanical properties.

A series of TEM measurements were carried out on the polymer composite comprising the coated $BaTiO_3$ to determine whether the nanoparticles are distributed uniformly throughout the PMMA matrix. Fig. 5 shows the TEM micrographs at different magnifications for the FG-PMMA-BT(PEDOT:PSS) sample (see Table 1). The sample preparation prior to TEM measurements included ultramicrotoming a very thin PMMA-ceramic section sitting on top of the fiberglass threads, at the outer surface. The $BaTiO_3$ nanoparticles are clearly visible in both micrographs, where the gray background represents the PMMA matrix. Although the SEM micrograph for the coated $BaTiO_3$ particles (Fig. 3c and d) indicated an agglomeration of the nanostructures in the powdery form, the low magnification TEM image (Fig. 5a) indicates an excellent distribution of the coated $BaTiO_3$ nanoparticles in the PMMA matrix. From the high magnification image (Fig. 5b) it is apparent that the nanoparticles range in size from about 80 nm to 100 nm.

3.3. Thermo-mechanical analysis of PMMA-composites

Fig. 6 shows the TGA (a) and derivative TGA (DTGA, (b)) data as a function of temperature for the three composite samples. For comparison, TGA and DTGA results from a reference, neat PMMA sample are also shown. From the TGA results it is apparent that addition of either neat or coated $BaTiO_3$ nanoparticles to the composites increases the decomposition temperature of PMMA. However, it is not very clear from the TGA plot (Fig. 6a) how the fiberglass alone impacts the decomposition temperature of PMMA. This feature is readily observable in the DTGA plot (Fig. 6b); it can be seen that the PMMA decomposition occurs at a higher temperature in the presence of fiberglass (maximum at 342 °C) compared to when PMMA is analyzed in the neat form (maximum at 300 °C). All decomposition peaks in the DTGA plot are accompanied by broad shoulders. The $BaTiO_3$ filler and/or fiberglass residue values

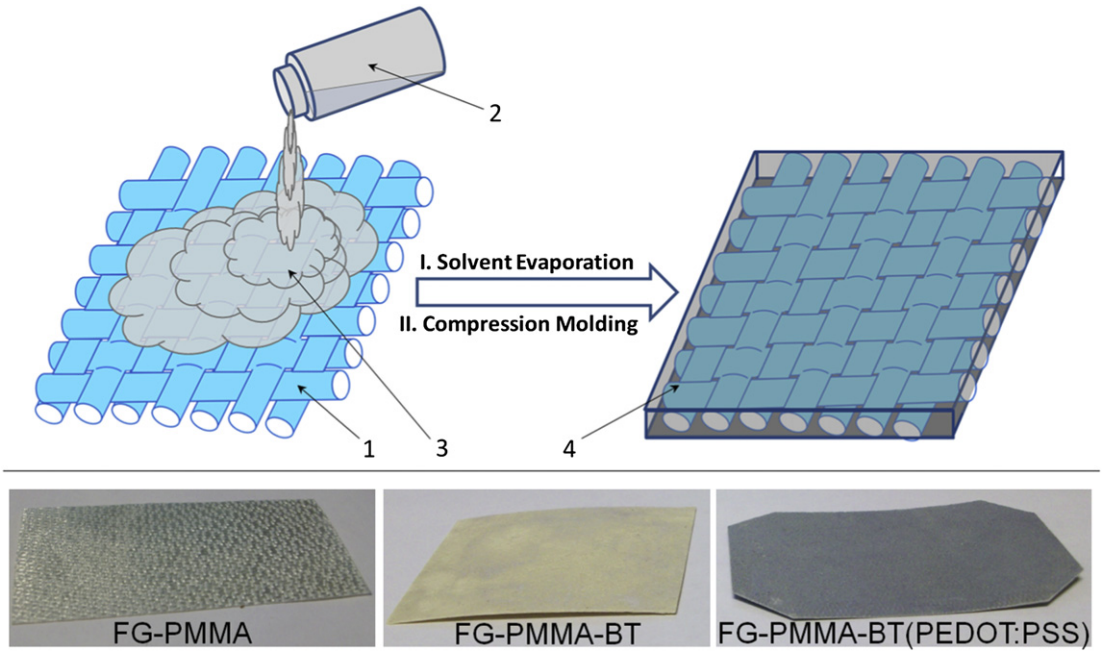

Fig. 4. The schematic (upper panel) shows the fabrication of PMMA-based composites containing fiberglass and particulate filler $BaTiO_3$. The components are: 1 – fiberglass mesh, 2 – vial containing the PMMA-filler dispersion in chloroform, 3 – PMMA-filler dispersion in chloroform, 4 – final PMMA-based composite containing fiberglass and particulate filler $BaTiO_3$. The lower panel presents pictures of the three composite films described in Table 1.

(%) from the combustion of the polymeric samples are in a good agreement with the filler amounts weighed during sample preparation (Fig. 6a).

Fig. 7a and b shows the storage modulus (E′) and loss tangent (tan δ) of the PMMA-composites, as a function of temperature, respectively. The DMA curves were obtained from rectangular-shaped samples subjected to a heating cycle with a rate of 3 °C/min at a frequency of 1 Hz. It is clear that the composite samples containing either neat or coated $BaTiO_3$ nanoparticles exhibit high E′ values. However, even in the absence of $BaTiO_3$ (i.e., FG-PMMA sample) the storage modulus is quite high, exhibiting a room temperature value of around 4 GPa. As expected, all polymeric samples experience a decrease of the storage modulus at elevated temperatures, but the decrease is not very drastic. For example, the FG-PMMA sample exhibits a storage modulus of around 2 GPa at 130 °C. The most important features obtained from the tan δ curves are the glass-transition temperatures (T_g) of the polymeric systems, taken as the temperature where the tan δ value is maximum (Fig. 7b). The T_g is observed to increase with addition of the $BaTiO_3$ nanoparticles to the composites. This trend is highly reproducible. Of course, another possibility would be to consider the T_g as the onset value where the storage modulus, E′, starts the sudden decrease. While the "tan δ method" indicates the point where all the polymer chains have reached the T_g, the "E′-onset method" indicates the point where the shorter polymeric chains have reached the T_g.

Improvement in the resistance to degradation of polymers with addition of fillers and/or fibers is typically attributed to the barrier effect that the fillers/fibers provide, as they slow down the volatilization processes of low-molecular weight products from the polymer degradation [33]. Consequently, it was not surprising that the temperatures corresponding to the main degradation peaks in the DTGA plot (Fig. 6b) increased with addition of fiberglass and $BaTiO_3$ nanoparticles. The three steps that are typically observed

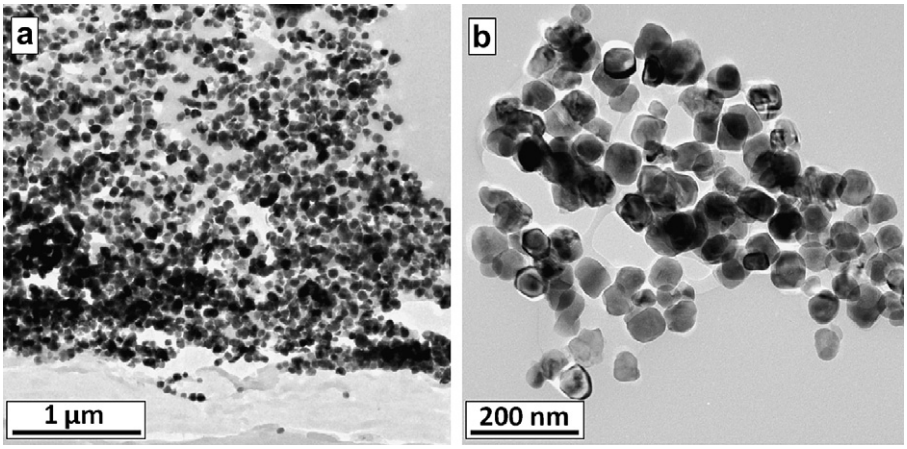

Fig. 5. TEM images at two distinct magnifications for the FG-PMMA-BT(PEDOT:PSS) sample (see Table 1).

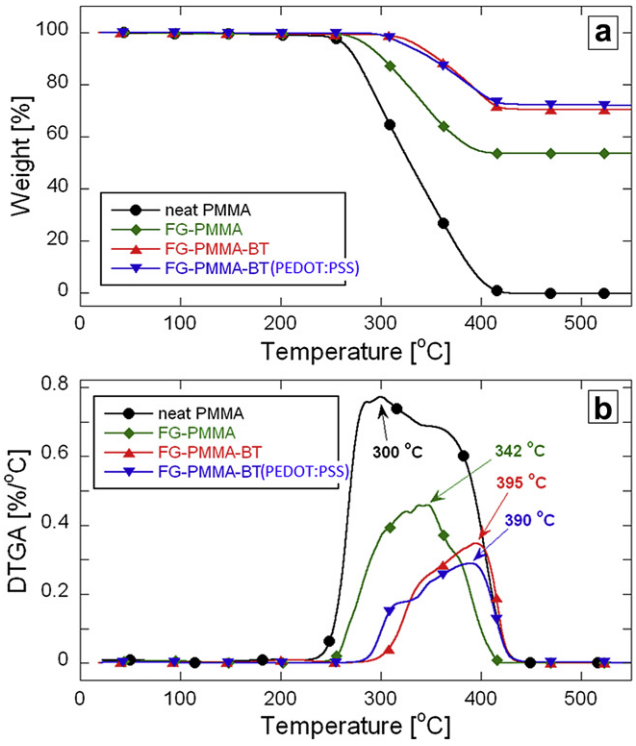

Fig. 6. TGA (a) and derivative TGA (b) data as a function of temperature for the neat PMMA and for the three composite samples. The heating rate was 20 °C/min in all measurements.

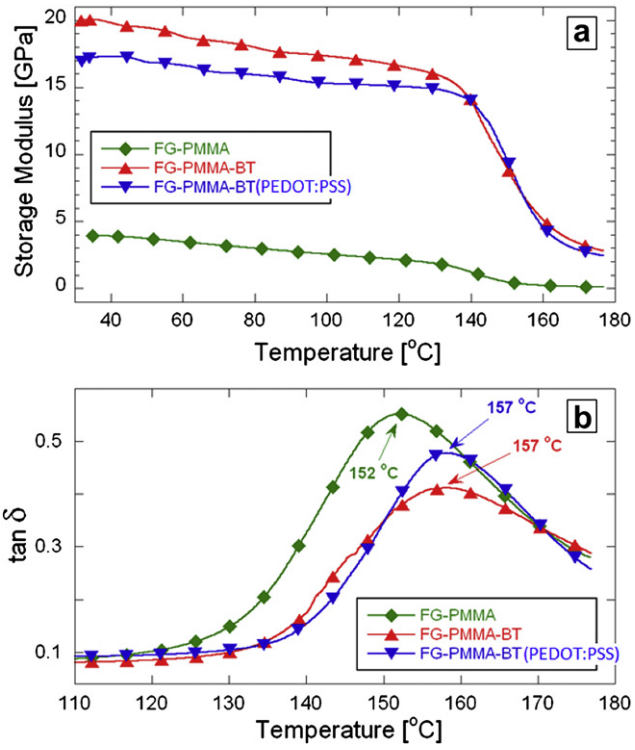

Fig. 7. Storage modulus (a) and tan δ (b) results as a function of temperature for the three PMMA-based composite samples, obtained from DMA measurements. The heating rate was 3 °C/min.

when neat PMMA is degraded in N_2 atmosphere, which have been previously attributed to head-to-head linkages, end-chain saturations and random chain scission [17], cannot be easily detected in the TGA trace obtained from the PMMA degradation in air (Fig. 6a). The presence of broad shoulders around the decomposition peaks in the DTGA plot, however, suggests that the three distinct processes observed in N_2 atmosphere are also present when the decomposition is conducted in air, where they might occur faster and be partially concomitant.

The increase in the stiffness and T_g of PMMA-composites with addition of fibers and/or various ceramic fillers has been observed and heavily reported in the literature [20,21,34]. The increase in the T_g with addition of fillers and/or fibers is primarily attributed to a decrease in mobility of the polymer chains owing to the confinement of macromolecules to the surface of the fillers and/or fibers. Furthermore, the stiffness increase can be primarily attributed to the stiffness of the filler and/or fiber, which are both several orders of magnitude higher than that of the pure polymer [35,36]. We have recently shown that, in the absence of the fiberglass fabric, $CaCu_3Ti_4O_{12}$-loaded PMMA-composites never exceed a storage modulus value of 2 GPa at room temperature [33]. Comparing that with the storage modulus of the FG-PMMA sample, observed in this work (Fig. 7a), it can be concluded that the fiberglass fabric brings a much higher contribution than the ceramic filler to the overall increase in stiffness. At a first glance this observation might appear counterintuitive, since the two $BaTiO_3$-containing samples, FG-PMMA-BT and FG-PMMA-BT(PEDOT:PSS) exhibit much higher stiffness than the $BaTiO_3$-free sample, i.e., FG-PMMA. However, in the absence of the fiberglass fabric, those samples would exhibit storage modulus values below 2 GPa, at room temperature.

While the $BaTiO_3$ reinforced samples exhibited significantly higher stiffnesses than the FG-PMMA samples, they exhibited tensile strengths which were statistically similar. The average tensile strength (of 4 independent samples) for the FG-PMMA was 208 ± 26.8 MPa, while the average tensile strength for the FG-PMMA-BT(PEDOT:PSS) sample was 222.8 ± 12.7 MPa, indicating that the strength of the composite samples is predominately dictated by the glass fiber, and is not significantly influenced by the presence of the $BaTiO_3$ nanoparticles.

3.4. Dielectric analysis of PMMA-composites

The dielectric constant, ϵ', and dissipation factor, tan δ (tan $\delta = \epsilon''/\epsilon'$), measured at room temperature (25 °C) for the polymer composites studied here are displayed in Fig. 8a and b, respectively. The electric field was applied perpendicular to the plane of the fiberglass mesh. The dielectric constant of the FG-PMMA sample ($\epsilon' \approx 6$–7) varied only slightly with frequency, barely decreasing as the frequency was elevated by six orders of magnitude. Addition of neat $BaTiO_3$ increased the dielectric constant of the material to around 14, without changing significantly the frequency dependence trend. At the same time, the dissipation factor trend of the FG-PMMA-BT remained roughly the same as that of the FG-PMMA, except for frequencies below 10 Hz. Furthermore, the addition of PEDOT:PSS-coated $BaTiO_3$ was observed to further increase ϵ' values relative to those of FG-PMMA-BT, and significantly change the frequency dependence of ϵ'. For example, when compared to the ϵ' of FG-PMMA-BT at 1 MHz, the ϵ' of the FG-PMMA-BT (PEDOT:PSS) composite increases by1.5, but in contrast, at 1 Hz ϵ' increases by about 6. It should be noted that at 1 Hz the ϵ' of FG-PMMA-BT(PEDOT:PSS) is 3 times larger than ϵ' of FG-PMMA. In addition, the tan δ values increase when PEDOT:PSS-coated $BaTiO_3$ is present in the composites. Importantly, tan δ of the FG-PMMA-BT (PEDOT:PSS) sample stayed below 0.07 for the entire range of frequencies studied.

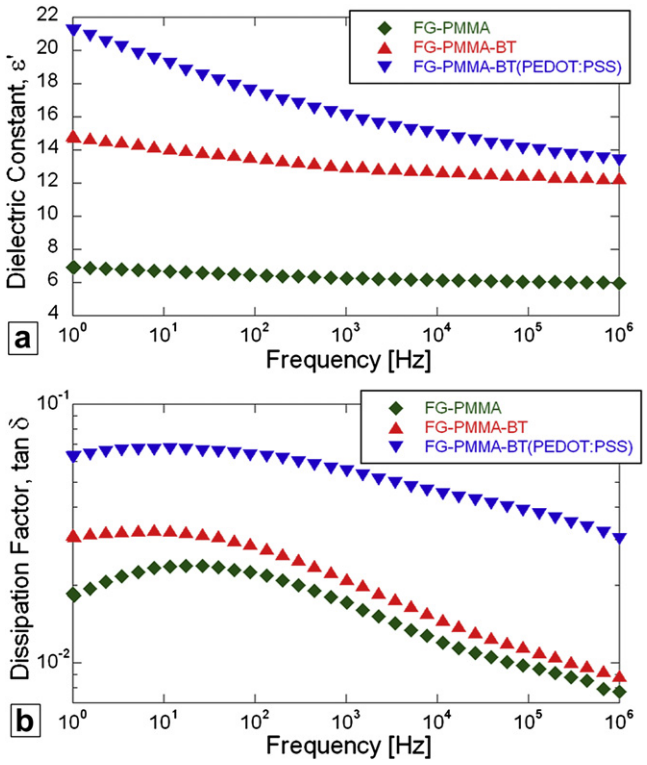

Fig. 8. Dielectric constant (a) and dissipation factor (b) data as a function of frequency for the three PMMA-composite samples.

In addition, Table 1 shows the breakdown voltage values for the three polymer composites. Each value was obtained by calculating the mean of five individual measurements conducted on each composite. The breakdown voltage values have been normalized for a thickness of 1 cm to allow comparison of results. It can be observed that the breakdown voltage values decrease in the order FG-PMMA > FG-PMMA-BT > FG-PMMA-BT(PEDOT:PSS). Moreover, the average size of the breakdown area in the tested samples was observed to decrease with addition of the neat and coated $BaTiO_3$ filler (see Supporting Information). Although the addition of neat $BaTiO_3$ is observed to lower the breakdown voltage of the composite, the decrease is not at all significant (Table 1). This minor reduction of the breakdown voltage may be attributed to a small increase in the density of defects in the volume of the polymer composite with addition of the neat nanoparticulate powder. On the other hand, the addition of PEDOT:PSS-coated $BaTiO_3$ is observed to significantly lower the breakdown strength voltage. In the case of the FG-PMMA-BT(PEDOT:PSS) sample the dominant factor responsible for the decrease of the breakdown voltage is the presence of free ions from PEDOT:PSS at the surface of nanoparticles, which imparts some electronic conductivity to the sample.

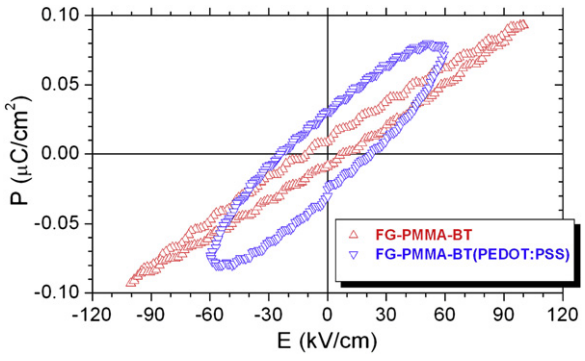

Fig. 9. Polarization vs. electric field hysteresis loops for the two PMMA-composites.

In order to elucidate the differences in the dielectric behavior between the FG-PMMA-BT and FG-PMMA-BT(PEDOT:PSS) samples, a set of polarization measurements on the two composites were performed. Fig. 9 shows the polarization hysteresis loops as a function of electric field for the FG-PMMA-BT and FG-PMMA-BT (PEDOT:PSS) samples. The FG-PMMA-BT(PEDOT:PSS) composite displayed a relatively large leakage current under strong electric fields (≤60 kV/cm) as demonstrated by the elliptical shaped loop. The curve for the FG-PMMA-BT composite appears in a much more linear fashion with minimum hysteretic behavior. In addition, it can be seen that this FG-PMMA-BT sample was able to withstand stronger electric fields (≤100 kV/cm). The results suggest that when the $BaTiO_3$ particles are coated with the conductive PEDOT:PSS blend, upon the incorporation in PMMA-composites the dielectric constant is enhanced at the expense of increased leakage current. The polarization vs. electric field results presented in Fig. 9 are in good accordance with the tan δ and dielectric breakdown voltage results shown in Fig. 8b and Table 1, where the dissipation factor of composites is observed to increase, and the breakdown voltage to decrease, due to the presence of PEDOT:PSS-coated $BaTiO_3$ particles.

Fig. 10 shows the temperature-dependent ϵ' and tan δ traces for FG-PMMA (a and b), FG-PMMA-BT (c and d), and FG-PMMA-BT (PEDOT:PSS) (e and f), respectively, as a function of frequency. The temperature in all measurements was elevated from −50 °C to +100 °C in 25 °C increments. For all three polymeric composites, higher temperatures resulted in elevated ϵ' and tan δ values. In the case of the FG-PMMA sample, ϵ' and tan δ vary only slightly with temperature. For example, at 1 MHz ϵ' increases by less than 0.3 as the temperature increases from −50 °C to +100 °C, and at 1 Hz the increase in ϵ' is approximately 1 over the same temperature range. For the FG-PMMA-BT sample, a slightly stronger frequency dependence of ϵ' is observed at elevated temperatures, and particularly at low frequencies. More precisely, at 1 MHz, ϵ' increases by less than 0.7 as the temperature is elevated from −50 °C to +100 °C, whereas at 1 Hz ϵ' increases by approximately 2.5. Additionally, for the FG-PMMA and FG-PMMA-BT composites tan δ values remain below 0.04 (<4%) for the entire range of frequencies at all temperatures studied. On the other hand, for the FG-PMMA-BT(PEDOT:PSS) composite, an even stronger frequency dependence of ϵ' over the temperature range from −50 °C to +100 °C is observed. For this sample at 1 MHz, ϵ' increases by nearly 1.3 as the temperature is elevated from −50 °C to +100 °C, whereas at 1 Hz ϵ' increases by about 5. Moreover, tan δ values of the FG-PMMA-BT(PEDOT:PSS) composite stay below 0.08 (<8%) over the entire range of frequencies at all tested temperatures.

It has been previously suggested that the increase of ϵ' with addition of ferroelectric ceramic powders, e.g., $BaTiO_3$, is primarily caused by the dipolar polarization effect induced by the permanent dipoles existent in the filler [33]. In the case of $BaTiO_3$, the permanent dipoles result from the uneven distribution of the charge-density between O, Ba and Ti atoms. For the FG-PMMA-BT (PEDOT:PSS) composite, the presence of PEDOT:PSS coating at the surface of $BaTiO_3$ particles introduces not only additional dipoles, but also ions, e.g., $-SO_3^-$. For this reason, in the FG-PMMA-BT (PEDOT:PSS) sample the dipolar polarization is complemented by ionic polarization [37,38], and the ϵ' values are, therefore, larger than those of the composite containing equal amounts of neat $BaTiO_3$ (Figs. 8a and 10c,e). In addition, owing in part to this complementary ionic polarization, in Fig. 9 the P values for the FG-PMMA-BT(PEDOT:PSS) sample appear larger than those of the FG-PMMA-BT sample at any given electrical field (E) in the range

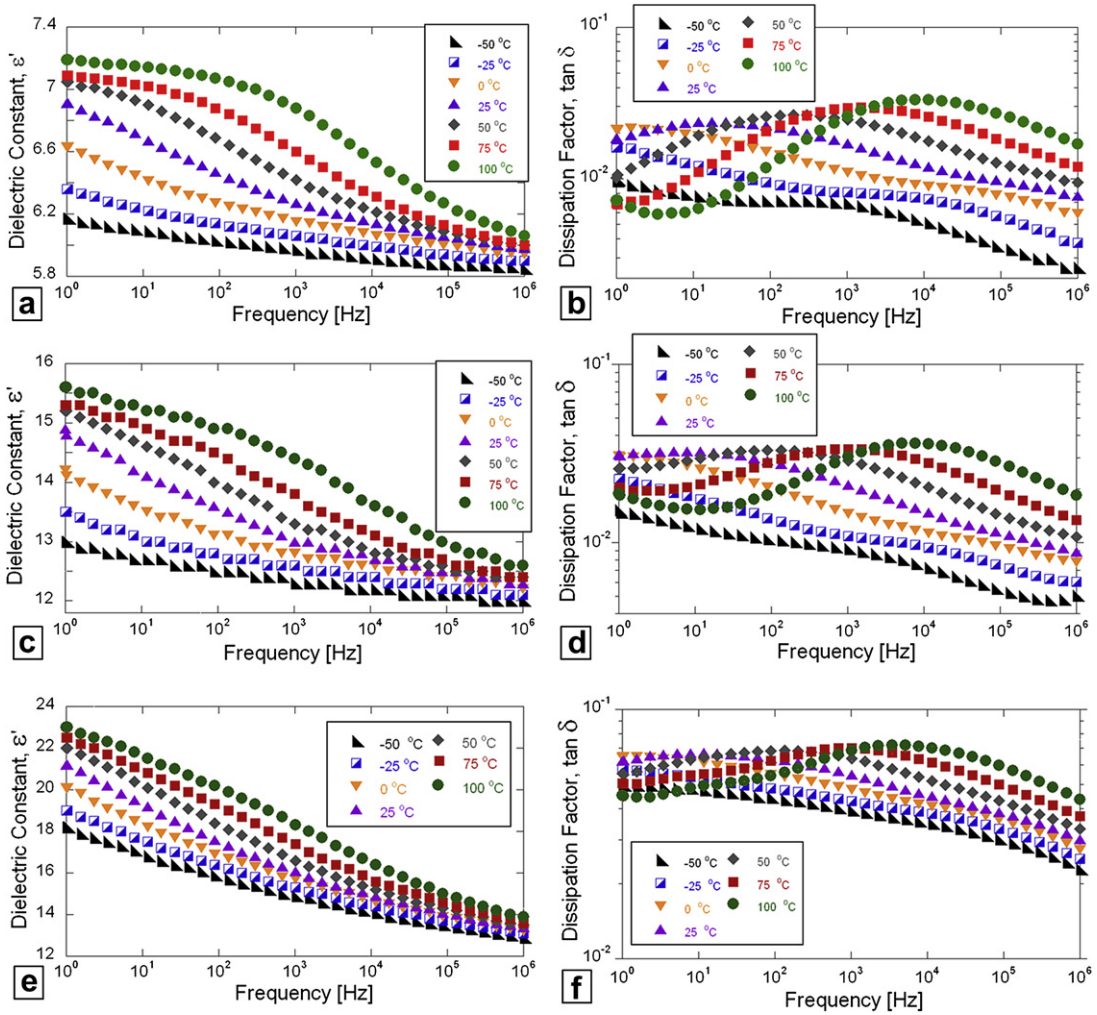

Fig. 10. Dielectric constant and dissipation factor for FG-PMMA (a and b), FG-PMMA-BT (c and d), and FG-PMMA-BT(PEDOT:PSS) (e and f), respectively, as a function of frequency at different temperatures.

0–60 kV/cm for the first quadrant and −60–0 kV/cm for the third quadrant. The FG-PMMA-BT sample, however, can withstand higher electrical fields due to its superior insulating characteristics (Fig. 9). In general, the dielectric dispersion of polymer composites, reflected in the frequency dependence of the ϵ' values, is typically attributed to complicated mechanisms relating to the existence of a lag between changes in polarization and changes in the electric field [39]. At frequencies in the range discussed here, induced atomic, electronic and/or ionic lattice polarizations are essentially instantaneous [18]. Only permanent molecular dipoles, ionic defects of dipolar type and low-mobility charge carriers have a non-instantaneous effect that contribute to the overall dielectric loss at these frequencies [40]. The dissipation factor decreasing with frequency has been previously attributed to the inability of the low-mobility charges to follow the applied time-varying field at high frequencies, resulting in a reduction of electronic oscillations [33]. In particular, the underlying relaxation observable in Fig. 10 is attributable to the β-relaxation in PMMA, due to localized oscillation of side groups attached to the polymer backbone.

Furthermore, the dielectric response of polymer composites at elevated temperatures is affected by several processes including mobility of ionic carriers, and development of space charges and polarization in the amorphous phase [41]. Upon heating, the combined action of those effects gives rise to an increase of dielectric permittivity of the polymer composite, even in the absence of the ceramic fillers (Fig. 10a). In the past, small variations of the dielectric constant and dissipation factor with temperature have been reported even for pure polymers [2,42]. Similar to the behavior of neat polymers, the FG-PMMA composite shows only a slight increase of the dielectric constant with temperature, which is most significant at low frequencies, as indicated in Fig. 10a. Although addition of neat and coated $BaTiO_3$ trigger a further increase of the dielectric constant and dissipation factor values at high temperatures (Fig. 10), our results suggest that these variations are quite small and that structural capacitors based on such polymer-based composite dielectrics may be useful in high-temperature-variation environments, particularly when utilized with high frequency alternating currents (AC). In addition, such structural capacitors may also be employed in high-temperature-variation environments when utilized for direct current (DC) applications, where the continuous nature of current doesn't cause the dipoles in the dielectric to vibrate and undesirably elevate the ion mobility or produce friction-induced effects such as local heating [2].

4. Conclusions

Achieving high stiffness in polymeric dielectrics of capacitors is often restricted by the competing need for high dielectric constants.

While high dielectric constant thermoplastic polymers, for example, poly(vinylidene fluoride) (PVDF) are too soft and flexible for structural applications, stiff thermoplastic matrixes, such as PMMA, have low dielectric constants. To achieve multifunctional structural capacitors requires the implementation of polymer-based composite dielectrics that exhibit superior mechanical properties and high dielectric constants. In this work we showed that PMMA-fiberglass structural dielectrics containing neat and PEDOT:PSS-coated $BaTiO_3$ are valuable potential dielectric candidates for multifunctional capacitor applications. Owing primarily to the presence of the fiberglass mesh, the ceramic-containing systems described here exhibit high storage modulus values, in excess of 15 GPa, for an extended range of temperatures (30–130 °C). Moreover, these composites exhibit good dielectric constants for a wide range of frequencies (1 Hz–1 MHz). Addition of PEDOT:PSS-coated $BaTiO_3$ particles was found to elevate the dielectric constant relative to that of the composites containing similar amounts of neat $BaTiO_3$. The high stiffness and dielectric constant values of the composites could be attributed in part to the excellent dispersion of the ceramic particles throughout the polymeric matrix, as evidenced by TEM. The presence of the ceramic filler was found to also improve (increase) the decomposition temperature and glass-transition temperature of the polymeric matrix in PMMA-fiberglass composites. The polymer-based composite dielectrics described here may be useful in environments where the temperature fluctuates anywhere between −50 °C and 100 °C, particularly when utilized in high frequency alternating currents (AC) or direct current (DC) applications.

Acknowledgments

This work is supported by NASA (Cooperative Agreement No.NNX09AP70A). The authors thank C. Stefanescu of LSU for help with the FTIR measurements. Special thanks are extended to Dr. Olesya Zhupanska for her support and thoughtful discussion and to Hongyu Cui for her help with the tensile testing experiments.

Appendix. Supplementary material

Supplementary data related to this article can be found online at doi:10.1016/j.polymer.2011.02.050.

References

[1] George S, Sebastian MT. Composites Science and Technology 2009;69 (7–8):1298–302.
[2] Kaiser CJ. The capacitor handbook. Olathe: CJ Publishing; 1995. p 133.
[3] Lavall RL, Borges RS, Calado HDR, Welter C, Trigueiro JPC, Rieumont J, et al. Journal of Power Sources 2008;177(2):652–9.
[4] Zhang Y, Feng H, Wu XB, Wang LZ, Zhang AQ, Xia TC, et al. International Journal of Hydrogen Energy 2009;34(11):4889–99.
[5] Ming-Jen P, Randall CA. Electrical Insulation Magazine, IEEE 2010;26(3):44–50.
[6] Manjunatha CM, Taylor AC, Kinloch AJ, Sprenger S. Journal of Reinforced Plastics and Composites 2010;29(14):2170–83.
[7] Manjunatha CM, Sprenger S, Taylor AC, Kinloch AJ. Journal of Composite Materials 2010;44(17):2095–109.
[8] Hautamaki M, Meretoja VV, Mattila RH, Aho AJ, Vallittu PK. Journal of Materials Science-Materials in Medicine 2010;21(5):1685–92.
[9] Weaver KD, Stoffer JO, Day DE. Polymer Composites 1995;16(2):161–9.
[10] Akat H, Tasdelen MA, Prez FD, Yagci Y. European Polymer Journal 2008;44 (7):1949–54.
[11] Chen-Yang YW, Lee YK, Chen YT, Wu JC. Polymer 2007;48(10):2969–79.
[12] Dhibar AK, Mallick S, Rath T, Khatua BB. Journal of Applied Polymer Science 2009;113(5):3012–8.
[13] Khatana S, Dhibar AK, Ray SS, Khatua BB. Macromolecular Chemistry and Physics 2009;210(13–14):1104–13.
[14] Kobayashi Y, Kurosawa A, Nagao D, Konno M. Polymer Engineering & Science 2009;49(6):1069–75.
[15] Kumar S, Rath T, Khatua BB, Dhibar AK, Das CK. Journal of Nanoscience and Nanotechnology 2009;9(8):4644–55.
[16] Lin R-Y, Chen B-S, Chen G-L, Wu J-Y, Chiu H-C, Suen S-Y. Journal of Membrane Science 2009;326(1):117–29.
[17] Oral A, Tasdelen MA, Demirel AL, Yagci Y. Polymer 2009;50(16):3905–10.
[18] Singh NL, Shah S, Qureshi A, Singh F, Avasthi DK, Ganesan V. Polymer Degradation and Stability 2008;93(6):1088–93.
[19] Wu T, Xie T, Yang G. Journal of Applied Polymer Science 2010;115(5): 2773–8.
[20] Goto K, Hashimoto M, Takadama H, Tamura J, Fujibayashi S, Kawanabe K, et al. Journal of Materials Science-Materials in Medicine 2008;19(3):1009–16.
[21] Boger A, Bisig A, Bohner M, Heini P, Schneider E. Journal of Biomaterials Science-Polymer Edition 2008;19(9):1125–42.
[22] Nasr GM, Ahmed RM. Modern Physics Letters B 2010;24(9):911–9.
[23] Choudhury A. Materials Chemistry and Physics 2010;121(1–2):280–5.
[24] Xie SH, Zhu BK, Wei XZ, Xu ZK, Xu YY. Composites Part a-Applied Science and Manufacturing 2005;36(8):1152–7.
[25] Yang Y, Nogami M, Shi JL, Chen HR, Ye LC, Qian SX. Journal of Materials Chemistry 2003;13(12):3026–32.
[26] Park JM, Lee HY, Kim JJ, Park ET, Chung YK. IEEE Transactions on Ultrasonics Ferroelectrics and Frequency Control 2008;55(5):1038–42.
[27] Chen L, Yuan CZ, Dou H, Gao B, Chen SY, Zhang XG. Electrochimica Acta 2009;54(8):2335–41.
[28] Daniel A, Fotheringham A. Journal of Applied Polymer Science 2007;104 (1):234–7.
[29] Mendez JD, Weder C. Macromolecular Chemistry and Physics 2008;209 (19):1960–6.
[30] Mendez JD, Weder C. Abstracts of Papers of the American Chemical Society 2008;235:131 [POLY].
[31] Nabid MR, Asadi S, Shamsianpour M, Sedghi R, Osati S, Safari N. Reactive & Functional Polymers 2010;70(1):75–80.
[32] Ohlan A, Singh K, Chandra A, Dhawan SK. Acs Applied Materials & Interfaces 2010;2(3):927–33.
[33] Stefanescu EA, Tan X, Lin Z, Bowler N, Kessler MR. Polymer 2010;51 (24):5823–32.
[34] Jancar J, Hynstova K, Pavelka V. Composites Science and Technology 2009;69 (3–4):457–62.
[35] Dong L, Stone DS, Lakes RS. Applied Physics Letters 2010;96(14).
[36] Salekeen S, Jones DL. Composite Structures 2007;79(1):119–24.
[37] Deepa M, Awadhia A, Bhandari S. Physical Chemistry Chemical Physics 2009;11(27):5674–85.
[38] Izgorodina EI, Forsyth M, MacFarlane DR. Physical Chemistry Chemical Physics 2009;11(14):2452–8.
[39] Kapustianyk V, Shchur Y, Kityk I, Rudyk V, Lach G, Laskowski L, et al. Journal of Physics-Condensed Matter 2008;20(36).
[40] Jonscher AK. Nature 1977;267(5613):673–9.
[41] Kelarakis A, Hayrapetyan S, Ansari S, Fang J, Estevez L, Giannelis EP. Polymer 2009;51(2):469–74.
[42] Venkat N, Dang TD, Bai Z, McNier VK, DeCerbo JN, Tsao B-H, et al. Materials Science and Engineering: B 2009;168(1–3):16–21.